

NON-LINEAR COMBUSTION STABILITY PREDICTION OF SRMS USING SPP/SSP

Jonathan French*, Software and Engineering Associates, Carson City, NV

ABSTRACT

Solid rocket motors experience combustion stability problems when the interior acoustic modes become coupled with combustion processes. Current linear stability analysis codes can predict if a solid rocket motor will be unstable, but do not predict the severity of the problem. Two non-linear analytic approaches have been devised that predict the limiting pressure amplitudes of these unsteady motions. The first approach is based upon numerically solving a system of ordinary differential equations in time. The second approach presumes the final relationship between the acoustic mode shapes, the combustion processes and the losses in the system. The basic theory behind each approach is presented, followed by the waveforms predicted for three different chamber configurations, including the Advanced Solid Rocket Motor. Both of these approaches rely on an accurate determination of the linear problem, and recent improvements to this analysis are presented as well.

INTRODUCTION

Solid rocket motor combustion instability occurs when combustion processes inside the rocket motor become coupled with the acoustic modes of the combustion chamber. The JANNAF Standard Stability Prediction program (SSP) was developed to predict SRM stability. It can only predict if a motor might be unstable, as it is based on a linear stability analysis of the motor. Once a motor goes unstable, it can either explode or enter a limited amplitude pressure cycle, in which the pressure oscillates about a DC pressure shift. Prediction of the maximum pressure amplitude requires a non-linear analysis of the interaction between the combustion processes and the acoustics of the combustion chamber.

Two approaches are examined in this paper. The first, developed by Culick¹, is an extension of the linear analysis. Culick's approach uses separation of variables to derive a system of ordinary differential equations (ODEs) composed of time-dependent amplitude functions (one per mode). The ODEs are linked due to non-linear gas dynamics and combustion response terms. The system can be integrated forward in time to predict the limiting amplitudes, or a bifurcation solver can be used to predict the limiting amplitude as a function of the unstable mode's overall exponential growth rate. The latter approach allows the analyst to evaluate the extent to which stability improvement is needed.

In Culick's model, no presumption is made as to the final relationship between the time varying functions. Culick's approach allows the amplitudes to float until they reach a "steady-state". However, the waves do coalesce into a recognizable pattern, as will be shown. The time integration approach (vs. the bifurcation method) has been implemented in SEA's SPP/SSP code set. The grain design and ballistics (SPP) and the linear stability analysis (SSP) can now feed information to the non-linear analysis without user intervention.

In contrast, Flandro^{2,3} has noted that the final form of the oscillatory flow commonly reduces to a traveling steeply fronted wave. In order to take advantage of this observation, he has utilized the Fourier decomposition of a traveling shock wave as the final relationship between the amplitudes and phase shifts of the acoustic waves. The presumption of the final form allows for an additional energy loss due to a gain in entropy across the traveling shock waveform, as predicted by Tempkin⁴. Despite the significant formulation differences between Culick and Flandro's models, these two approaches yield similar results. We will compare and contrast results between these two approaches in this paper.

An underlying similarity between these approaches is their reliance on the linear stability analysis. The linear stability alphas (and in Culick's approach the linear phase shift) are significant parameters in both Culick

Copyright © 2003 by Software and Engineering Associates, Inc. Published by the American Institute of Aeronautics and Astronautics, Inc., with permission.

*Jonathan French, Senior Engineer, AIAA Member

and Flandro's analyses. Therefore, if meaningful results are desired, an accurate evaluation of the linear stability analysis is required before attempting a non-linear analysis. To this end, we have made several improvements to the linear stability analysis found in the SPP/SSP code set. These improvements and their results shall be presented first.

LINEAR STABILITY IMPROVEMENTS

The non-linear combustion stability analysis is highly dependent on the accuracy of the linear stability analysis. In this section we present our improvements to the linear SSP algorithm. The SSP code itself has changed very little since its incorporation into SPP in 1987,⁶ and the fundamental underlying routines are robust. We have recently re-examined SSP, and improved the acoustic solver and the SPP/SSP linkage. These stability improvements are evaluated using the ASRM test case (see Figure 4).

SSP Acoustic Theory Improvements

While SSP contains arrays that allow for the mean density and acoustic velocity to vary axially, the 1987 SPP/SSP linkage sets the density and speed of sound to axially constant values. There appears to be a problem with the derivation of the acoustic mode solver in SSP that prevents the use of an axially varying mean density. The code uses the mean density to compute the acoustic velocity, so it is an important parameter. In this section we derive a corrective modification to SSP.

The acoustic mode solver uses an "exponential horn" geometrical approximation in order to use an analytic solution for an axial wave in a duct with a changing cross-sectional area.⁵ The ODE is

$$\frac{d}{dz} \left[S(z) \frac{dp'}{dz} \right] + S(z) k^2 p' = 0 \quad (1)$$

The exponential horn approximation uses an analytic expression for the cross-sectional area:

$$S(z) = S_{I,1} e^{a_I z} \quad (2)$$

$$a_I = \ln(S_{I,2}/S_{I,1})/L_I$$

The general solution to this equation is:

$$p'_I(z) = e^{-a_I z/2} [A_I f_i(k_I z) + B_I g_i(k_I z)] \quad (3)$$

$$\begin{array}{ll} f_i & g_i \\ k^2 > 0 & \cos(kz) \quad \sin(kz) \\ k^2 < 0 & \cosh(kz) \quad \sinh(kz) \end{array}$$

SSP allows the user to define adjacent axial segments, and assumes the mean density and speed of sound is constant across each segment as shown in Figure 1:

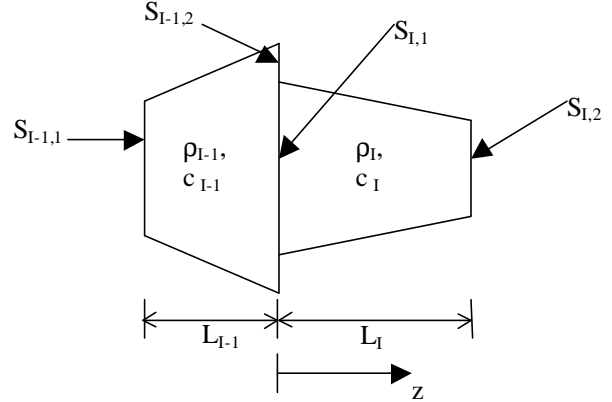


Figure 1. Adjacent Motor Segments in SSP

SSP uses equation (3) to model the acoustics across segments, and matches the pressure and the volumetric flow rate at the interface between segments.⁶ From the continuity of volumetric flow assumption, replacing the acoustic velocity with the perturbed pressure terms:

$$\begin{aligned} u'_{I-1,2} S_{I-1,2} &= u'_{I,1} S_{I,1} \\ u' &= \frac{i}{r w} \frac{\partial p'}{\partial z} \\ \frac{1}{r_{I-1}} \frac{\partial p'_{I-1,2}}{\partial z} S_{I-1,2} &= \frac{1}{r_I} \frac{\partial p'_{I,1}}{\partial z} S_{I,1} \\ \frac{\partial p'_{I,1}}{\partial z} &= \frac{r_I S_{I-1,2}}{r_{I-1} S_{I,1}} \frac{\partial p'_{I-1,2}}{\partial z} \end{aligned} \quad (4)$$

SSP assumes that the pressure at the interface is continuous:

$$p'_{I,1} = p'_{I-1,2} \quad (5)$$

Alternately, for duct acoustics, Dowling and Ffowcs Williams recommend using continuity of mass and energy at discontinuities.⁷ This introduces a slight change to the solution, but we will insert a parameter so either assumption may be applied, and compare the results.

From mass conservation at the interface between the segments:

$$\begin{aligned} \mathbf{r}_{I-1} u'_{I-1,2} S_{I-1,2} &= \mathbf{r}_I u'_{I,1} S_{I,1} \\ u' &= \frac{i}{\mathbf{r} \mathbf{w}} \frac{\partial p'}{\partial z} \\ \frac{\partial p'_{I-1,2}}{\partial z} S_{I-1,2} &= \frac{\partial p'_{I,1}}{\partial z} S_{I,1} \\ \frac{\partial p'_{I,1}}{\partial z} &= \frac{S_{I-1,2}}{S_{I,1}} \frac{\partial p'_{I-1,2}}{\partial z} \end{aligned} \quad (6)$$

From conservation of energy at the interface:

$$\begin{aligned} p'_{I-1,2} u'_{I-1,2} S_{I-1,2} &= p'_{I,1} u'_{I,1} S_{I,1} \\ p'_{I,1} &= \frac{u'_{I-1,2} S_{I-1,2}}{u'_{I,1} S_{I,1}} p'_{I-1,2} \end{aligned} \quad (7)$$

Again, from conservation of mass:

$$\begin{aligned} \mathbf{r}_{I-1} u'_{I-1,2} S_{I-1,2} &= \mathbf{r}_I u'_{I,1} S_{I,1} \\ \frac{\mathbf{r}_I}{\mathbf{r}_{I-1}} &= \frac{u'_{I-1,2} S_{I-1,2}}{u'_{I,1} S_{I,1}} \\ p'_{I,1} &= \frac{\mathbf{r}_I}{\mathbf{r}_{I-1}} p'_{I-1,2} \end{aligned} \quad (8)$$

This approach leads to an extra ratio of the steady density terms from each side of the interface. To add this ratio as a parameter to the conservation solution, let:

$$\begin{aligned} \mathbf{b} &= \frac{\mathbf{r}_I}{\mathbf{r}_{I-1}} \\ p'_{I,1} &= \mathbf{b} p'_{I-1,2} \\ \frac{\partial p'_{I,1}}{\partial z} &= \frac{1}{\mathbf{b}} \frac{\mathbf{r}_I S_{I-1,2}}{\mathbf{r}_{I-1} S_{I,1}} \frac{\partial p'_{I-1,2}}{\partial z} \end{aligned} \quad (9)$$

The mass and energy conservation approach allows us to vary the density on a per-segment basis. As the variation in the density is typically small between segments, \mathbf{b} is close to 1. However, as will be shown later, allowing the mean density to vary without accounting for conservation of mass and energy can lead to a significant error in the modal analysis.

SSP originally computed the mean axial velocity as a function of surface area exposure, burn rate, propellant density and gas density. The aft mean axial velocity is an important quantity, as the nozzle damping stability parameter is linearly proportional to it. SPP also computes this value in its ballistics module. When we compared the SPP and SSP axial mean velocities for several test cases, the mean velocities compared well

when the motors were axi-symmetric. However, we found significant differences when non-axi-symmetric motor designs were evaluated, due to 3D grain design mass addition. SPP now passes the ballistic computed mean velocity to SSP, and this modification has resulted in a significant change in the overall stability prediction of our ASRM test motor.

We also made a minor modification to the speed of sound. While the SPP/SSP linkage assumed the speed of sound was constant throughout the chamber, the SSP code is designed to allow for different speeds of sound on a segment by segment basis. Our new linkage computes the speed of sound locally as a function of the local mean density and mean pressure.

Geometry Resolution Improvements

The original SSP code required the user to specify the grain design and ballistics parameters manually for each web step under consideration. In 1987, SEA incorporated the SSP1D code into the SPP code, with the appropriate linkages to interpolate the SPP grain design and ballistics results onto 40 user selected fixed axial locations. This did not allow the SSP code to track burning radial slot locations.

We have recently developed a new linkage which allows SSP to use the same axial stations as found in SPP, so geometry and ballistics data are no longer interpolated from SPP to SSP. SPP contains a feature that allows it to shift the axial station locations to match radial slot positions as the slots burn back. These burning slot locations are now automatically passed to SSP.

The exponential horn approximation is purported to be accurate as long as the area ratio between the ends of segment is less than a factor of two.⁶ The perimeter is also approximated using the exponential horn relationship in order to yield analytic solutions to the stability integrals. To accommodate this limitation, if the areas are found to change too quickly across a segment, an additional axial station is inserted to split a single segment in two. The left segment and right segment areas are set to maintain a discontinuity at their interface. For example, for the rocket motor segment in Figure 2, the cross sectional area changes too quickly. To fix this, the segment is split in two and an additional axial station is inserted, as in Figure 3. When the motor contains an axial slot, the insertion of the additional axial station correctly tracks the slot location.

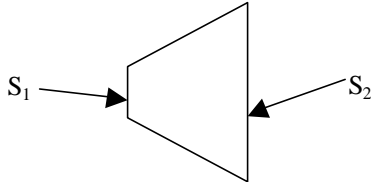


Figure 2. Sudden change in cross-sectional area (S) across a motor segment

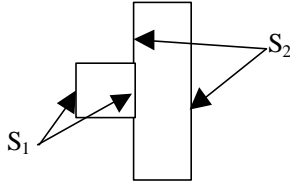


Figure 3. Sudden change in cross-sectional area (S) replaced by two discontinuous segments

ASRM Test Case

The ASRM test case grain design burn back is shown in Figure 4. The ASRM grain design consists of an 11-point star at the head end and two radial slots. We have used this motor to examine how our SPP and SSP improvements affected the computed stability, and have produced two sets of results. The first set examines how parameters vary axially at three different time steps during the motor burn. In this set of computations, results from the original SSP computation and the new SPP/SSP linkage are shown. The second set examines how the acoustics and stability parameters vary as a function of time. In the latter studies, axial variations in the mean density and speed of sound are also examined.

The effect of using all of SPP's axial stations in SSP is best seen in Figure 5. The source of the cross-sectional areas is identical for the old and new SSP linkages. The difference between the original and improved linkages is due to the increased number of axial stations used.

SEA has recently developed a highly accurate perimeter algorithm in SPP that computes both the burning and non-burning perimeters at each axial location. In our new SPP/SSP linkage, we now pass these burning and non-burning perimeters to SSP. Figure 6 compares the original ASRM SSP burning perimeters with the new perimeters at three separate times. The large head end perimeter (from head end fins) is distinctly visible in the computation for the new linkage in Figure 6a. The slot locations are also prominent, and as the slots burn out to the case, the burning perimeter goes to zero as seen in Figure 6b and Figure 6c.⁸

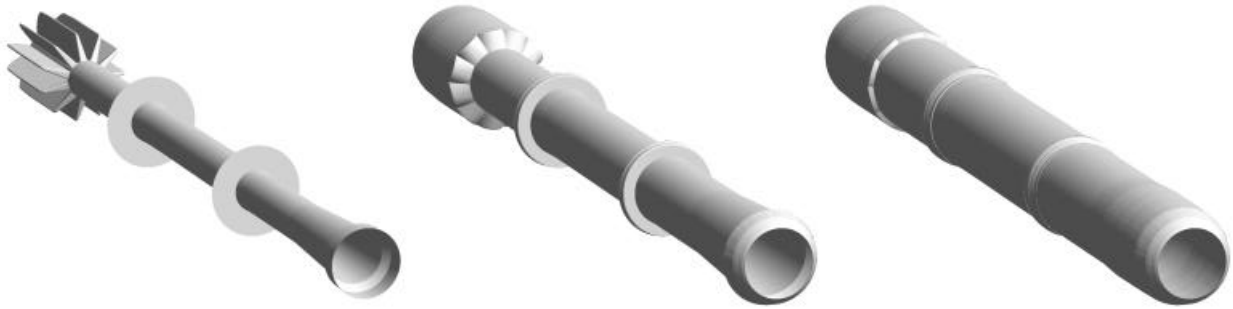
As the motor burns back, the pressure mode shapes vary only slightly between the original and new SSP linkages (Figure 7). However, the acoustic velocity computation shows a tremendous difference, especially early in the motor burn (Figure 8a).

The mean velocity shows a large change, again early in the burn. This is because the head end fins produce a large mass flux that the SSP mean velocity approximation cannot account for (Figure 9a). In particular, the aft end mean velocity changes significantly, which has a direct impact upon nozzle damping.

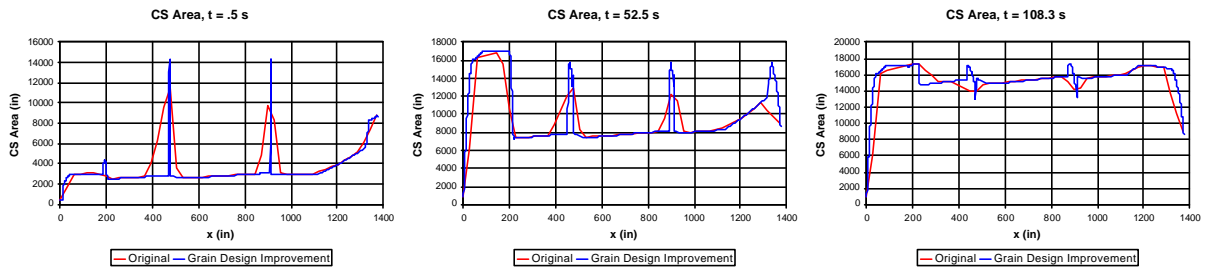
The second set of analyses examined how the frequency, the overall stability alpha and the individual stability alphas varied versus time with different new options enabled. In this analysis we compared the original SSP results with results produced using the new grain design linkage. In addition, we examined the effect of allowing the density to vary with the improved grain design option. With the axially varying density, we also examined turning on the density "fix" derived in a previous section, and allowing the speed of sound to vary. The last test turned on all of these options simultaneously.

It is evident from Figure 10a, which plots the variation in the first acoustic mode's frequency versus time, that the main improvement to the acoustics solver in SSP was the increased axial resolution of the parameters. All of the other modifications are second order effects compared to this change. In the stability analysis, it is apparent that the next most influential modification was the density variation. If the density is allowed to vary axially without implementing the "density fix", the early stability in Figure 10b diverges significantly from the improved grain design alone. However, once the density fix is implemented, the stability is much closer to the grain design improvement case by itself. It is also apparent that allowing the speed of sound to vary has no significant effect in any of the test cases.

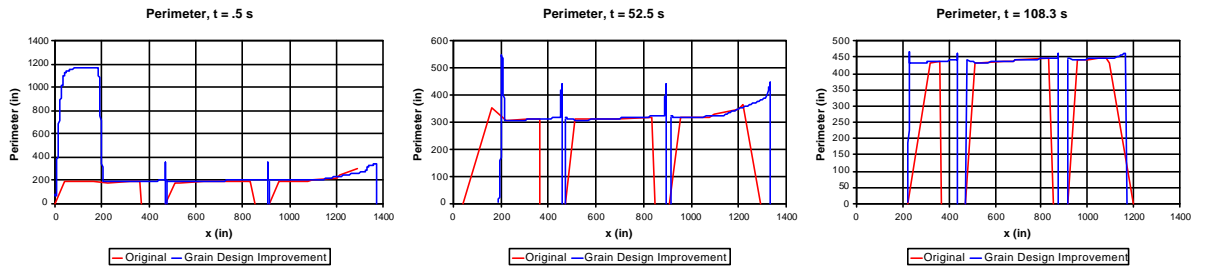
In the individual stability integrals, the pressure coupled response was dramatically increased during the initial burn, as a result of the improved perimeter calculation (Figure 10c). The other major change in the stability integrals was, as expected, in size of the nozzle damping term. This is important, as the nozzle damping term is a very significant damping term (Figure 10g).



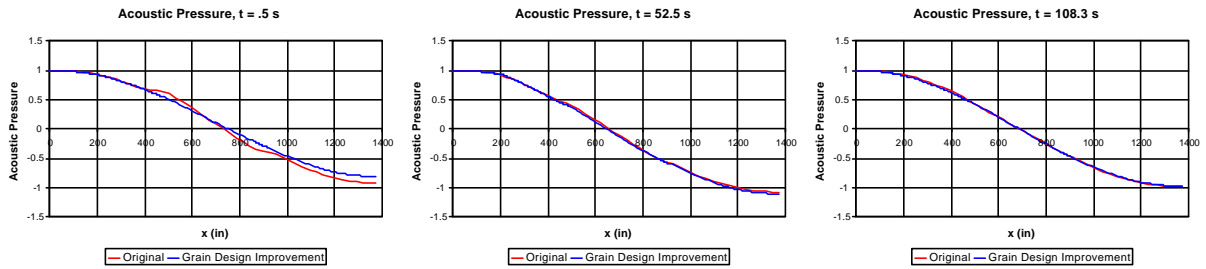
(a) Time = .5 seconds (b) Time = 52.5 seconds (c) Time = 108.3 seconds
 Figure 4. ASRM burn back at different time steps



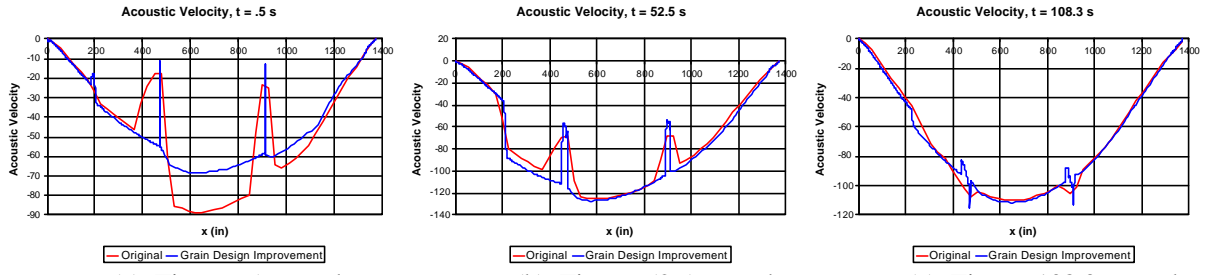
(a) Time = .5 seconds (b) Time = 52.5 seconds (c) Time = 108.3 seconds
 Figure 5. Comparison of original and improved grain design linkage effects on cross-sectional area



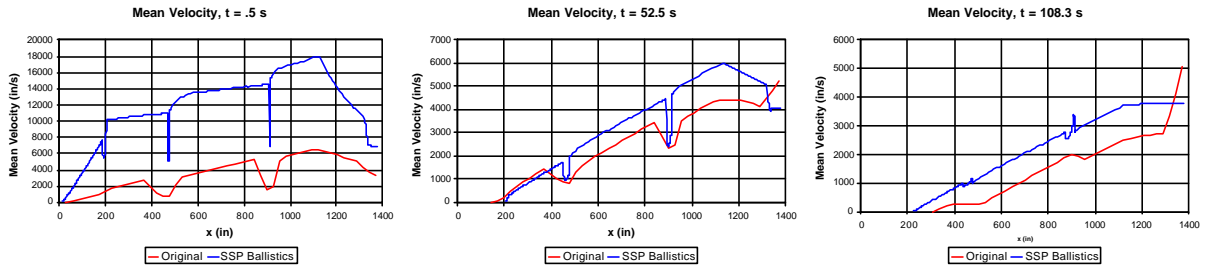
(a) Time = .5 seconds (b) Time = 52.5 seconds (c) Time = 108.3 seconds
 Figure 6. Comparison of original and improved grain design linkage effects on burning perimeter



(a) Time = .5 seconds (b) Time = 52.5 seconds (c) Time = 108.3 seconds
 Figure 7. Comparison of original and improved grain design linkage effects on acoustic pressure



(a) Time = .5 seconds (b) Time = 52.5 seconds (c) Time = 108.3 seconds
 Figure 8. Comparison of original and improved grain design linkage effects on acoustic velocity



(a) Time = .5 seconds (b) Time = 52.5 seconds (c) Time = 108.3 seconds
 Figure 9. Comparison of original SSP computed mean velocity and SSP ballistics mean velocity

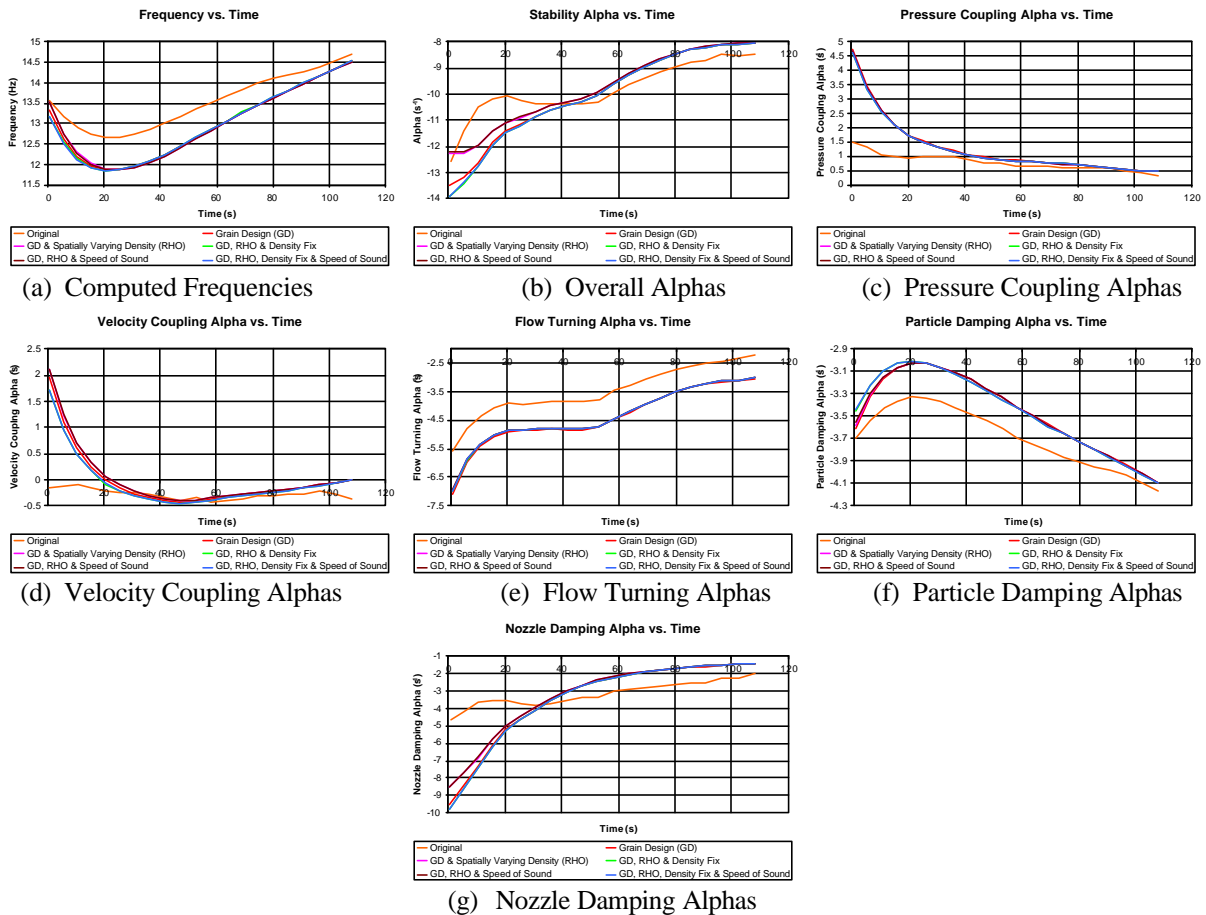


Figure 10. Effect of SSP modifications on stability

EVALUATION OF NON-LINEAR STABILITY METHODOLOGIES

Linear stability analysis is dependent only on spatial variables to determine if a SRM could be unstable. Non-linear analyses require a time component to determine the severity to which an unsteady motion could grow, as the linear unstable processes are damped by higher modes non-linear processes. Non-linear analyses of solid rocket motors have taken two forms: time accurate CFD simulations of the unstable motions, and analytic approaches relying on separation of variables to introduce a time component. Inclusion of a CFD approach within the SPP/SSP framework would be prohibitive in terms of both implementation and computational time. A multi-dimensional non-linear CFD code requires more information that SPP was designed to provide, and would be more properly implemented as a separate code. Also, SPP is a design code, implying that run times must be kept short or the code loses its utility. While CFD codes provide a direct perspective of the fluid motion, rather than by Fourier decomposition of the motion, such codes are currently best suited for validating results from the analytic methods.

Analytic approaches have been successfully implemented, and have produced results similar to the CFD codes. The analytic approach can also be embedded within the SPP/SSP framework, allowing the user to implement the analysis with a minimum of effort. The separation of variables assumption allows the spatial motions to be considered apart from the time variation of each mode shape. The mode shapes, already computed in SSP, are used to establish an ordinary system of equations in time. Once they are used to form weights driving the system of ODEs, they are no longer needed. They can later be used in conjunction with the time parameters to determine the overall motion of the fluid.

Culick's Non-Linear Approach

Culick's approach utilizes separation of variables directly. We have followed the formulation from Burnley⁹ in developing our SPP/SSP implementation. The partial differential equation of interest is the wave equation:

$$\begin{aligned} \frac{1}{\bar{a}^2} \int \mathbf{y}_n \frac{\partial^2 p'}{\partial t^2} dV + k_n^2 \int \mathbf{y}_n p' dV \\ = - \int \mathbf{y}_n h dV - \oint \mathbf{y}_n f dS \end{aligned} \quad (10)$$

Separation of variables is used to define the pressure as the sum of the product of the mode shape and its time varying function:

$$\frac{p'(\bar{r}, t)}{\bar{p}} = \sum_{m=1}^{\infty} \mathbf{h}_m(t) \mathbf{y}_m(\bar{r}) \quad (11)$$

$$u'(\bar{r}, t) = \sum_{m=1}^{\infty} \frac{\mathbf{h}_m(t)}{\bar{g} k_m^2} \nabla \mathbf{y}_m(\bar{r}) \quad (12)$$

The mode shapes () are already known. Thus, solving for :

$$\frac{\partial^2 \mathbf{h}_n}{\partial t^2} + \mathbf{w}_n^2 \mathbf{h}_n = - \frac{\bar{a}^2}{\bar{p} E_n} \left\{ \int \mathbf{y}_n h dV - \oint \mathbf{y}_n f dS \right\} \quad (13)$$

The parameters h and f contain the first and second order gas dynamics terms which drive the system of equations:

$$\begin{aligned} h = - \bar{\mathbf{r}} \nabla \cdot \left(\bar{\mathbf{u}} \cdot \nabla u' + u' \cdot \nabla (\bar{\mathbf{u}} - u') - \frac{p'}{\bar{g} \bar{p}} \frac{\partial u'}{\partial t} \right) \\ + \frac{1}{\bar{a}^2} \bar{\mathbf{u}} \cdot \nabla \frac{\partial p'}{\partial t} + \frac{\bar{\mathbf{g}}}{\bar{a}^2} \frac{\partial p'}{\partial t} \nabla \cdot \bar{\mathbf{u}} + \frac{1}{\bar{a}^2} \frac{\partial}{\partial t} (u' \cdot \nabla p') \\ + \frac{\bar{\mathbf{g}}}{\bar{a}^2} \frac{\partial}{\partial t} (p' \nabla \cdot u') + \nabla \cdot \mathbf{F}' - \frac{1}{\bar{a}^2} \frac{\partial P'}{\partial t} \end{aligned} \quad (14)$$

$$\begin{aligned} f = \bar{\mathbf{r}} \left(\frac{\partial u'}{\partial t} + \bar{\mathbf{u}} \cdot \nabla u' + u' \cdot \nabla \bar{\mathbf{u}} + u' \cdot \nabla u' \right) \cdot \hat{\mathbf{n}} \\ + \frac{p'}{\bar{a}^2} \frac{\partial u'}{\partial t} - \mathbf{F}' \cdot \hat{\mathbf{n}} \end{aligned} \quad (15)$$

The first order terms comprise the linear stability terms. When the first order terms are approximated with equations (11) and (12), the integrals of the product of two mode shapes (equation (13)) yield the Kronecker delta, because the mode shapes are orthogonal. The first order terms have only one time function, and as such are linear and may be placed on the left hand side (LHS). However, when the second order terms are approximated with equations (11) and (12), the product of three mode shape functions are integrated in space, yielding a third order tensor dotted with two time function vectors. These two time function vectors represent the non-linear portion of the ODE, and are placed on the right hand side (RHS) to drive the linear LHS:

$$\begin{aligned} \ddot{\mathbf{h}}_n - 2\mathbf{a}_n \dot{\mathbf{h}}_n + (\mathbf{w}_n^2 - 2\mathbf{w}_n \mathbf{q}_n) \mathbf{h}_n = \\ - \sum_{i=1}^{\infty} \sum_{j=1}^{\infty} [A_{nij} \mathbf{h}_i \mathbf{h}_j + B_{nij} \mathbf{h}_i \dot{\mathbf{h}}_j] \end{aligned} \quad (16)$$

A_{nij} and B_{nij} are 3rd order tensors which contain all the spatial effects (some terms have been presumed to be small and thus neglected):

$$A_{nij} = \frac{1}{E_n^2} \int \left\{ \frac{1}{\bar{g}k_i^2} (\nabla y_i \cdot \nabla y_j + \bar{g} y_j \nabla^2 y_i) y_n \right. \\ \left. + \frac{1}{\bar{g}k_i^2 k_j^2} [(\nabla y_i \cdot \nabla) \nabla y_j] \cdot \nabla y_n \right\} dV \quad (17)$$

$$B_{nij} = -\frac{1}{E_n^2} \int \left\{ \frac{\bar{a}^2}{\bar{g}} [(\nabla y_i \cdot \nabla y_j + \bar{g} y_j \nabla^2 y_i) y_n] \right. \\ \left. + y_i \nabla y_j \cdot \nabla y_n \right\} dV \quad (18)$$

The simplest approach to solving this system of equations (16) is to determine the stability alphas (\mathbf{a}_n) and phase shifts (\mathbf{q}_n) using SSP, imparting an initial amplitude for the unstable mode, and then integrating forward in time. There is also the bifurcation approach, which varies the unstable mode's alpha to provide the user with an idea of the global stability of motor, but this is not yet implemented in SSP. Also, SSP currently lacks the computation for the phase shift.

Flandro's Non-Linear Approach

Flandro's approach is similar, but contains a significant assumption: the final form of the overall wave motion is a steeply fronted traveling wave.^{2,3} The Fourier coefficients are selected to be a sawtooth wave front. Therefore, rather than allowing the spectral components to float towards a final solution, each is given a weight relative to the first mode. The only unknown is the overall amplitude of the summation of the modes. Rather than refer to the wave equation, Flandro implements an energy balance with sources of energy from the linear instability, such as pressure coupling, and a primary non-linear sink, identified as the entropy gain across the steeply fronted wave, as originally derived by Temkin⁴. The rate of energy dissipation across the steep wavefront (for a perfect gas) is:

$$\frac{\partial E_{steepwavefront}}{\partial t} = A_{cs} \frac{\bar{g} + 1}{2} \frac{(\Delta p')^3}{6 r_0^2 c_0^3} \quad (19)$$

$\Delta p'$ is the jump in the perturbed pressure across the steep wavefront. The motivation for this approach was to ensure that this entropy loss is incorporated into the solution, and to simplify the analysis procedure. Time integration or a bifurcation solution of a larger system of ODEs is no longer needed. Simplification of the problem also allows one to better understand the underlying physics of the problem. For a cylindrical motor, the energy balance, written in terms of the steeply fronted waveform's amplitude, can be written as:

$$\frac{de}{dt} = e \mathbf{a}_1 - e^2 \left(\frac{\bar{g} + 1}{6\bar{g}} \right) \frac{\bar{a}}{L} \quad (20)$$

wherein L is the cylinder length, \bar{a} is the speed of sound, \bar{g} is the ratio of the specific heats, and \mathbf{a}_1 is the first mode's stability parameter.

Comparison of Results

In developing test cases, we had two goals in mind: validate our current Culick based analysis, and examine the overall fluid motion to evaluate the accuracy of Flandro's steeply fronted wave assumption. Two particularly useful set of test cases were obtained from the studies of Dennison and Baum¹⁰ and Baum and Levine¹¹. They performed CFD simulations of unsteady motions, and developed numerical techniques to capture steeply fronted fluid motions with a minimum of dissipation. Herein we have compared Culick and Flandro's analytic methods with the CFD results of Baum and Levine for both a cylinder and two cylinders with a sudden area change. This is then followed by a fictitious evaluation of the unsteady motions within the ASRM test motor.

Cylindrical Motor Case

The cylindrical test case was the primary example provided in Culick and Yang¹, in which Culick's approach was compared with CFD results from Dennison and Baum. The time evolution of the overall amplitude of the instability from Culick's analysis is shown in Figure 11, and the spectral component evolution is shown in Figure 12. When Baum and Levine's CFD results were Fourier decomposed, they matched Culick and Yang's amplitudes well (see Table 1). Our SSP results (based on Burnley's derivation⁹) match Culick and Yang's results as well (see Figure 13). It should be noted that these results are only for five acoustic modes, and that additional modes can be included in the analysis (at the expense of additional computational effort).

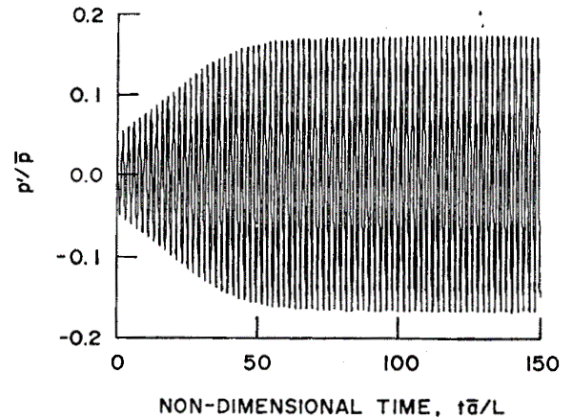


Figure 11. Computed limit cycle (Culick's method)

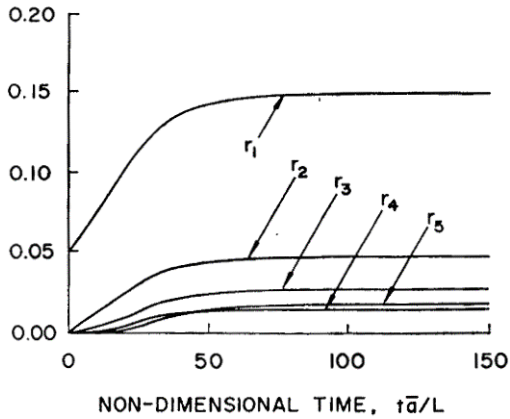


Figure 12. Spectral variation (Culick)

Table 1. Comparison of computed acoustic mode amplitudes

Mode	Pressure (p'/p)		
	Baum & Levine	Culick & Yang	SSP & Time Integration
1	0.151	0.151	0.151
2	0.042	0.0478	0.0483
3	0.0234	0.0280	0.0284
4	0.0203	0.0153	0.0153
5	-----	0.0188	0.0192

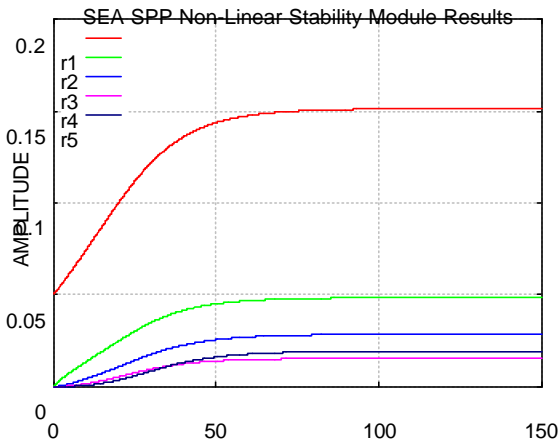


Figure 13. Spectral variation (SSP)

When examining solutions to problems that have been Fourier decomposed, it is important to remember that the overall solution is the superposition of the modes. When evaluating results, often the pressure time history for one location is presented, as in Figure 11. It is helpful to examine axial plots of the perturbed pressure at different time steps during the periodic motion. Figure 16 contains eight time slices of the perturbed fluid motion, using three different approaches. As can be seen in the first column of Figure 16, the overall

solution found from Culick's approach is a steeply fronted, albeit not sharp, traveling wave front. Culick's analysis is dependent on the linear stability alphas, but Culick and Yang only provided the stability alphas for the first five modes. We took the liberty of generating 15 additional fictitious but reasonable stability alphas, providing a total set of 20 modes which were used to repeat the computation for the cylinder (see Table 2). The inclusion of the additional modes removed spurious oscillations in the unsteady motion as can be seen in the second column of Figure 16. The corresponding spectral variation is shown in Figure 14.

Flandro's approach yields a normalized limiting pressure amplitude of 0.149, which matches the overall amplitude computed by Dennison and Baum in Figure 11. This value was computed by integrating equation (20) in time until a limit cycle was reached (see Figure 15). For comparison purposes, Flandro's sawtooth waveform is provided in the third column of Figure 16, but the amplitudes were not adjusted to match the problem. The ripples in Flandro's solution are due to the truncation of the sawtooth waveform at 20 modes. As more waves are added, the waveform becomes smoother.

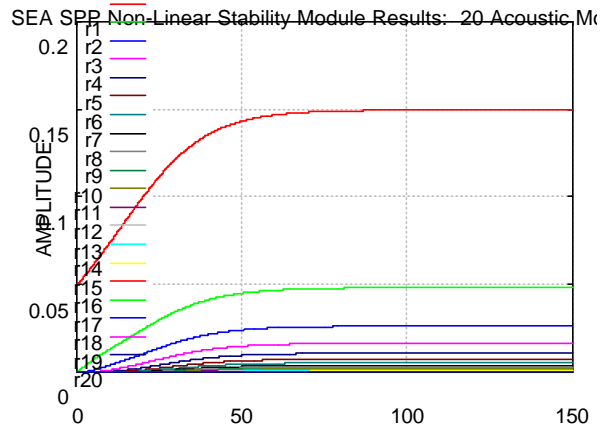


Figure 14. Spectral variation (SSP, 20 modes)

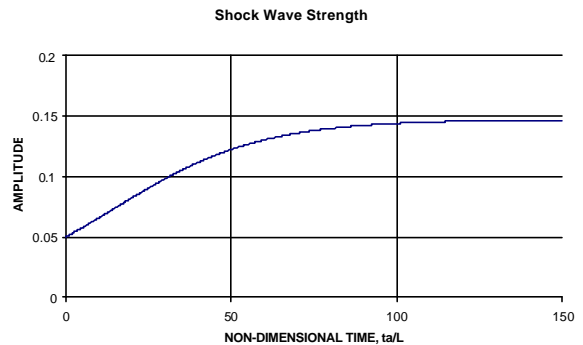


Figure 15. Limiting Amplitude (Flandro)

In this example, the stability alphas and phase shifts were taken from Culick and Yang¹. SSP has not been programmed to compute the phase shifts. Out of curiosity, we changed the phase shift values from Culick and Yang to all zeros and random values, with no appreciable change to the final results. This bodes well, as the phase shift combustion response parameter (the imaginary portion of the combustion response function) is a difficult parameter to obtain, and would reduce the amount experimental effort required if it could be ignored. Modification of the stability alpha does yield significant changes, but fortunately this parameter can be obtained using T-burner experiments.¹²

Stepped Area Duct Case

Many solid rocket motors are not strictly cylindrical in nature, so it is important to evaluate these motors using more complicated grain designs. After the cylinder, Baum and Levine's stepped area duct case (see Figure 17) is a simple test case that can easily be evaluated using both Culick and Flandro's methods. The original plots from Baum and Levine¹¹ are reproduced in the first column of Figure 18. In the stepped area duct, a steeply fronted wave traveling from the left to the right is transmitted to the larger region, and an expansion fan is reflected. When a steeply fronted wave travels from the right to the left, part of the wave is transmitted and part of the wave is reflected. The original purpose of this test problem was to demonstrate Baum and Levine's CFD code's lack of dissipation of shock wave fronts. In their CFD analysis, the flow field was excited with a continuous disturbance of the first axial mode with the pressure fluctuation equaling 20% of the mean pressure. However the flow field quickly took on steeply fronted wave characteristics.

As Baum and Levine do not make note of the stability alphas and phase shifts, we utilized the same parameters as used in the cylindrical test case (Table 2) for our analysis using Culick's model. Culick's approach returns similar results, but the waveform is greatly dissipated. As we do not know what the correct stability parameters are, this is not unexpected. On the contrary, we were pleased to note that we were able to reconstruct a similar waveform. In contrast, Flandro's approach yields a waveform that is sharper than that found in the CFD solution. This was not entirely expected. We used the same sawtooth waveform as that used for the cylinder, and it is apparent that the Fourier coefficients are the same for the cylinder and the stepped duct.

Culick (5 modes) Culick (20 modes) Flandro (20 modes)

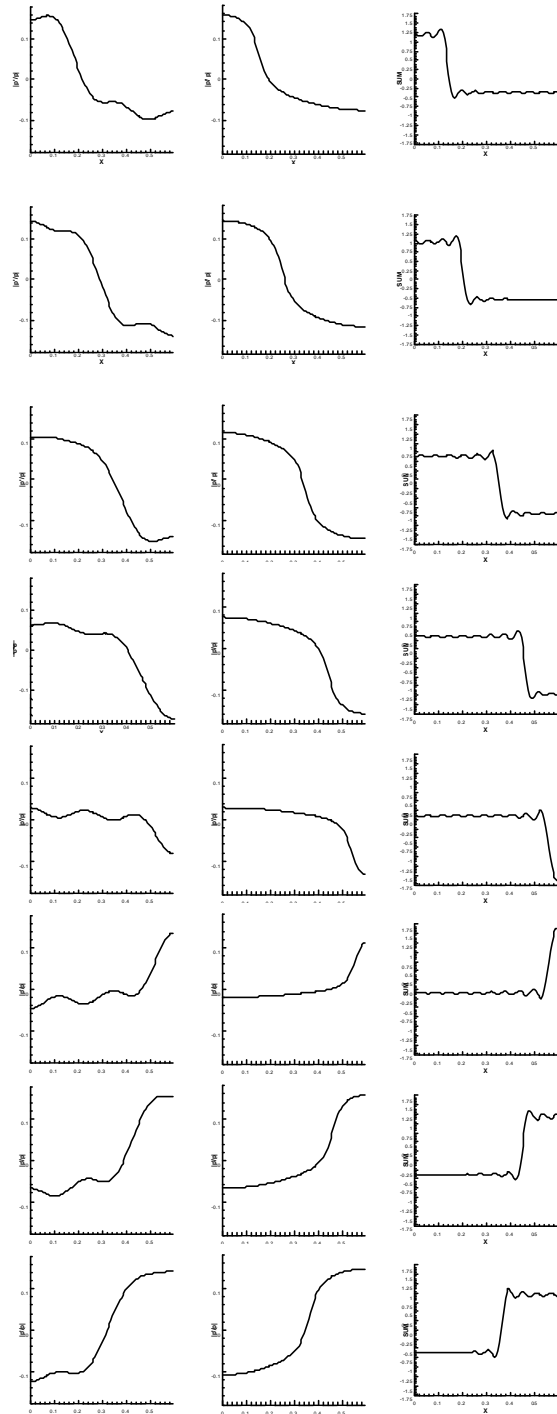


Figure 16. Comparison of pressure distribution histories for cylinder

Table 2. Mode stability alphas and thetas

Mode	1	2	3	4	5	6	7	8	9	10	11	12	13	14	15	16	17	18	19	20
	81.4	-316	-561	-874	-1256	-1637	-2019	-2401	-2782	-3164	-3546	-3928	-4309	-4691	-5073	-5454	-5836	-6218	-6599	-6981
	34.8	101	118	197	335	473	611	749	888	1026	1164	1302	1440	1579	1717	1855	1993	2131	2270	2408

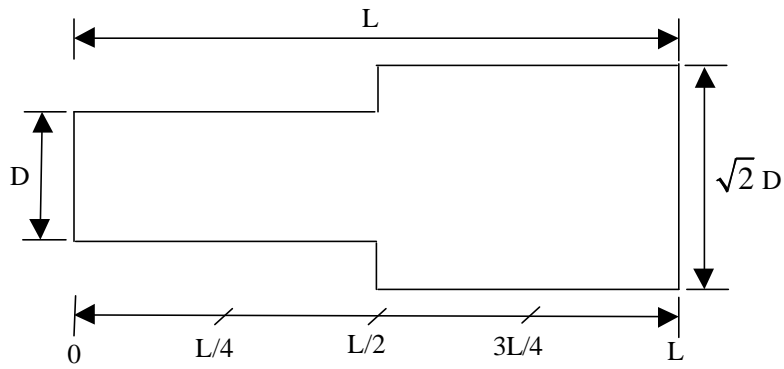


Figure 17. Stepped Area Duct Geometry

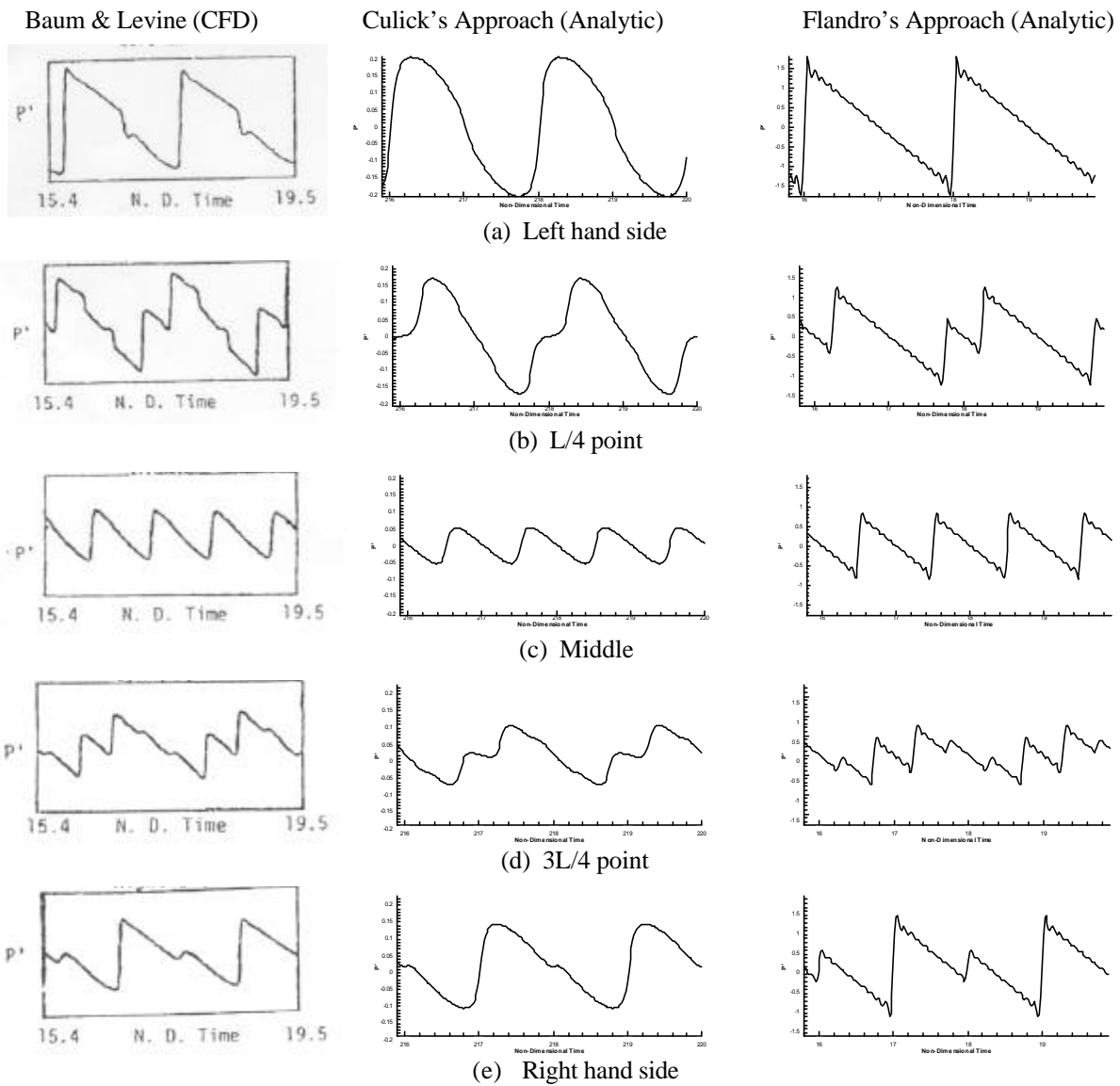


Figure 18. Comparison of Results from Baum & Levine¹¹, Culick and Flandro

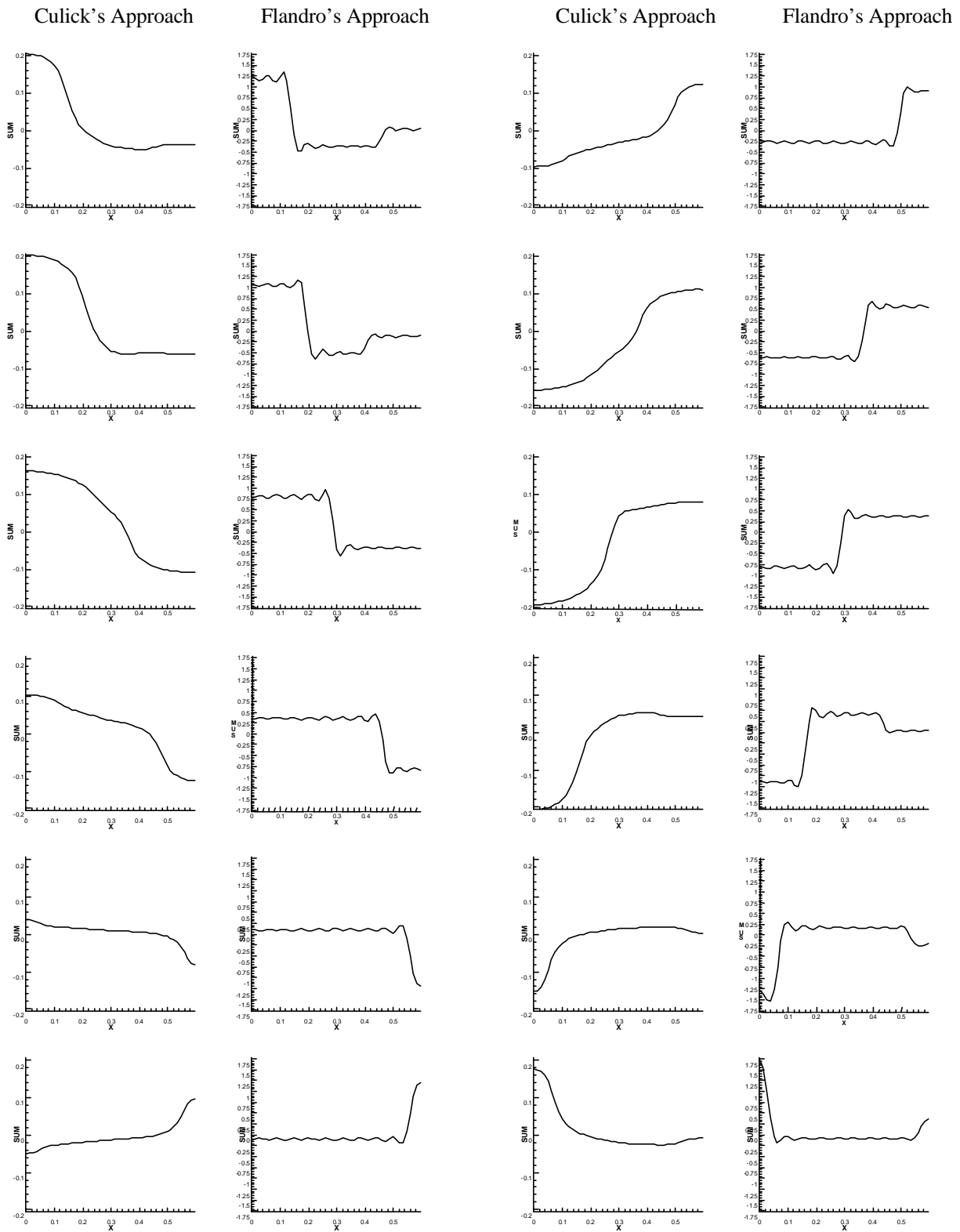


Figure 19. Comparison of perturbed pressure distribution histories for stepped area duct

ASRM Test Case

The ASRM motor test case demonstrates how a generic motor geometry can be modeled. As we did not have a set of stability alphas or phase shifts for the ASRM, we utilized the stability parameters of the Dennison and Baum¹⁰ cylindrical test case. The stability alphas were multiplied by ratios of the chamber lengths and speeds of sound to determine reasonable values for this significantly different problem:

$$\mathbf{a}_{ASRM,i} = \frac{L_1 c_2}{L_2 c_1} \mathbf{a}_{cylinder,i} = 0.01683 \mathbf{a}_{cylinder,i} \quad (21)$$

As can be seen in Figure 20, similar results were achieved: a steeply fronted traveling wave was produced. These figures were generated using Culick's approach for the motor geometry at 25.4 seconds into the burn. Several of the figures show the left end of the axial pressure plot maintaining a flat profile – this is due to the fins in the head end burning out, resulting in a larger cross sectional cylinder in the head end of the motor.

Flandro's approach produces a single traveling wave to the right, after which the waveform dissolves into random motions. Culick's approach has a built in control loop, whereas Flandro's approach requires extremely accurate mode shapes in order to maintain a repeatable waveform. It is also possible that for non-cylindrical motors, a more complicated set of sawtooth weights is required.

CONCLUSIONS AND FUTURE WORK

We have greatly improved the SSP computations by improving the resolution of motor geometry, passing the axial mean velocity from SPP directly (rather than computing it in SSP) and allowing for spatial variation in the density.

Culick's approach has been successfully implemented as a module of SPP/SSP, with the mode shapes passed from SSP. The stability parameters were fixed, but the mechanisms are in place for these values to be passed from SSP as well. We successfully matched the Dennison and Baum cylindrical test case, and also applied the same algorithm against the a stepped area motor and the ASRM.

For the stability alphas used in Dennison and Baum, it appears that Flandro's assumption that the waves are steeply fronted is reproduced using Culick's approach.

Our current efforts include implementing Culick's bifurcation analysis, which determines the maximum amplitude of the system as a function of the unstable mode's alpha, and working with Flandro to formulate his analysis to predict the DC shift and triggering.

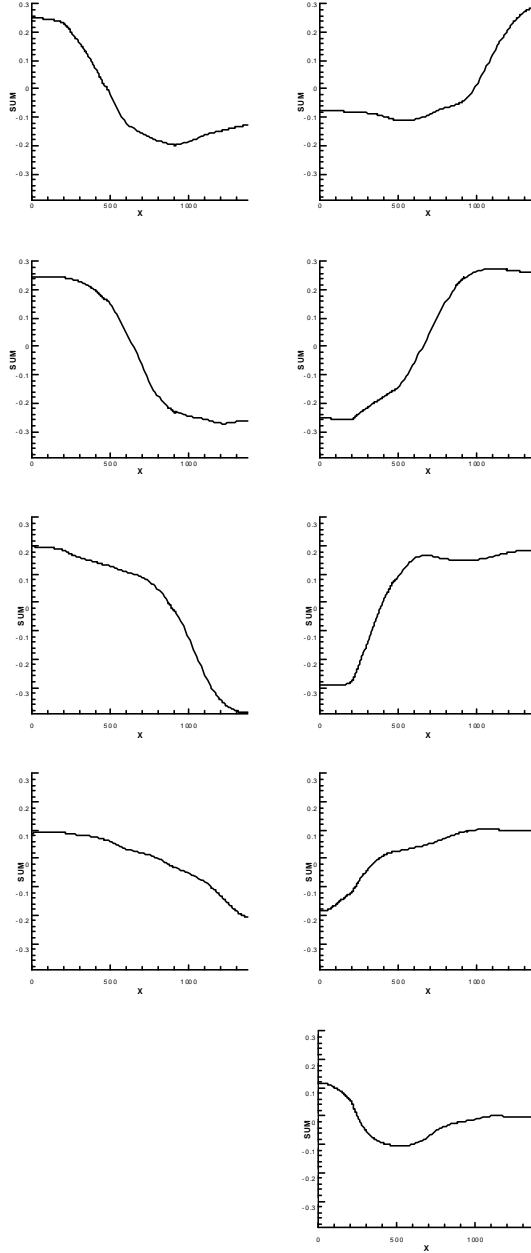


Figure 20. ASRM perturbed pressure distribution history

ACKNOWLEDGEMENTS

We would first like to thank Fred Blomshield, of NAWC / China Lake, for his support in funding this effort. This paper would not have been possible without the groundbreaking work performed by Fred Culick, in the development of the system of ODEs. We also appreciate the help from Gary Flandro for bringing to our attention the Baum and Levine¹¹ stepped area motor, and for comparing his approach with it, as well as for his insights into the underlying mechanisms of non-linear combustion stability.

-
- ¹ Culick, F.E.C., and Yang, V., "Prediction of the Stability of Unsteady Motions in Solid Propellant Rocket Motors", Chapter 18 in *Nonsteady Burning and Combustion Stability of Solid Propellants*, Progress in Astronautics and Aeronautics, Vol. 143, 1992.
 - ² Flandro, G.A., "Approximate Analysis of Nonlinear Instability with Shock Waves", AIAA-82-1220, 18th Joint Propulsion Conference, Cleveland, OH, June 1982.
 - ³ Flandro, G.A., "Energy Balance Analysis of Nonlinear Combustion Stability", *Journal of Propulsion and Power*, Vol 1, No 3, pp 210-221, May-June 1985.
 - ⁴ Morfey, C.L., Temkin, S., "Unstable Combustion of Advanced Solid Propellants", Bolt, Beranek and Newman, Inc., Report No. 1547, Contract No. DA-18-001-AMC-1134(X), September 1967.
 - ⁵ French, J.C., "Non-Linear Combustion Stability Prediction of Solid Rocket Motors", Phase I Final Report, prepared for Naval Air Warfare Center, China Lake, CA, Contract N68936-02-C-0018, May 2002.
 - ⁶ Nickerson, G.R., Culick, F.E.C., Dang, A.L., "The Solid Propellant Rocket Motor Performance Prediction Computer Program (SPP), Version 6.0, Volume VI: Standard Stability Prediction Method for Solid Rocket Motors, Axial Mode Computer Program User's Manual", Software and Engineering Associates, Inc., Carson City, NV 1976, p. 25.
 - ⁷ Dowling, A.P., Ffowcs Williams, J.E., "Sound and Sources of Sound", Ellis Horwood, Ltd., ©1983.
 - ⁸ Coats, D.E., French, J.C., Dunn, S.S., Berker, D.R., "Improvements to the Solid Performance Program (SPP)", AIAA-2003-4504, 39th AIAA / ASME / SAE / ASEE Joint Propulsion Conference, Huntsville, AL, July 2003.
 - ⁹ Burnley, V.S., "Nonlinear Combustion Instabilities and Stochastic Sources", Thesis, California Institute of Technology, CA, 1996.

-
- ¹⁰ Dennison, M.R., and Baum, E., "A Simplified Model of Unstable Burning in Solid Propellants," *American Rocket Society Journal*, Vol. 31, No. 8, 1961, pp.112-1122.
 - ¹¹ Baum, J.D., Levine, J.,N., "Modeling of Nonlinear Combustion Instability in Solid Propellant Rocket Motors," AFRPL TR-83-058, February 1984.
 - ¹² Culick, F.E.C., et al, "T-Burner Manual", CPIA Publication No. 191, November 1969.